Kinetic Evidence for a Monomer Activation Step in Actin Polymerization†

John A. Cooper,* E. Loren Buhle, Jr., Simon B. Walker, Tian Y. Tsong, and Thomas D. Pollard

ABSTRACT: We measured the time course of skeletal muscle actin polymerization at different actin concentrations. In 0.1 M KCl with 1 mM Mg^{2+}, log/log plots of the rate of the early, slow phase of polymerization vs. actin concentration were linear with slopes from 1.0 to 1.3. Computer-assisted calculations of similar curves from theoretical models with different sizes for the nucleus showed that no simple model gave a log/log plot with a slope less than 1.5. Addition of a first-order, monomer activation step before nucleation allowed models of any reasonable nucleus size to have a slope of 1. This is the first evidence that such a step is part of the kinetic pathway for actin polymerization. In 0.1 M KCl with 0.2 mM Ca^{2+}, log/log plots of the rate of the slow phase vs. actin concentration were linear with slopes from 2.0 to 2.5. Monomer activation was not necessary to account for this slope. However, fits of kinetic curves calculated from theoretical models to experimental kinetic curves showed that filament fragmentation was important to achieve a good fit, confirming the finding of Wegner and Savko [Wegner, A., & Savko, P. (1982) *Biochemistry 21*, 1909–1913]. Our fit procedure also allowed us to estimate the size of the nucleus and the rate constants for activation, nucleation, and fragmentation. In 0.1 M KCl with 1 mM Mg^{2+}, the nucleus was a dimer or trimer, and nucleation was fast. In 0.1 M KCl with 2.0 mM Ca^{2+}, the nucleus was a trimer, and nucleation was slow.

Several reversible reactions, including monomer activation, nucleation, elongation, and filament fragmentation, have been proposed as steps in the transition of actin monomers to polymers, which are characterically 7 nm wide helical filaments. Some of these steps have clearly been shown to exist, but others have not. Some of the steps are accessible to direct observation, which has enabled quantitative measurement of their parameters. For most of the steps, the parameters cannot be measured directly, however.

Monomer activation is a term used to describe changes in actin monomers caused by the monovalent or divalent ions that induce polymerization. It has not been shown to be a step in the polymerization scheme. There is ample evidence that actin monomers have a different conformation in polymerizing as opposed to nonpolymerizing conditions. This so-called "F-monomer" state has been detected by proteolytic susceptibility (Rich & Estes, 1976), fluorescence of an actin derivative (Frieden et al., 1980; Frieden, 1982), and ultraviolet absorption spectroscopy (Rouayrenc & Travers, 1981; Pardee & Spudich, 1982). A step such as salt binding to actin is a monomer activation step in the sense that it is first order with respect to actin concentration and is required for polymerization. However, this step might be so rapid as to be unimportant to the overall rate. The unanswered questions are whether any first-order steps including the transition to these F-monomer states are slow enough to be rate limiting during nucleation or elongation and whether any conformational changes in actin monomers affect polymerization by either (1) being a required step in the polymerization scheme or (2) altering the rate constants for monomer participation in subsequent polymerization steps. We report here the first evidence for a rate-limiting monomer activation step by analyzing the actin concentration dependence of the rate of the slow phase under one ionic condition.

Nucleation is the formation of an actin oligomer (nucleus) that can propagate the growth of an actin filament at the rapid rate characteristic of the elongation process. The formation of nuclei is highly unfavorable. Nucleation clearly exists, but its parameters are less well described. The critical concentration, or condensation, phenomenon displayed by actin is predicted by nucleated assembly but not by simple linear assembly without nucleation. For simple assembly, plots of monomer vs. total protein are smooth. As total protein increases, the monomer concentration approaches a limiting concentration. For nucleated assembly, plots of monomer vs. total protein are not smooth. They have a sharp corner at the critical concentration. This behavior is predicted by the model for nucleated polymerization described by Oosawa & Kasai (1962). The parameters describing nucleation are the size of the nucleus and the forward and backward nucleation rate constants. With certain assumptions, Oosawa & Kasai derived two equations that were used by Kasai et al. (1962) to measure experimentally the size of the nucleus. Their result was 3 to 4. The values of the nucleation rate constants have not been measured.

Elongation has been well documented. Two experiments show that monomers associate and dissociate at filament ends, but not sides. First, the monomer concentration never exceeds the critical concentration, regardless of the polymer concentration. This result is predicted by linear polymerization, both with and without nucleation. Second, the rate of growth from a single filament is constant with time, given a constant monomer concentration (Pollard & Mooseker, 1981). The rate would increase with time if monomers added along the side of a growing filament. The values of the elongation rate constants can be measured relatively accurately. First, the individual elongation rate constants for both association and dissociation at both barbed and pointed filament ends (as defined by the binding of myosin subfragment 1 to actin filaments) can be measured in an electron-microscopic assay (Pollard & Mooseker, 1981). Second, the ratio of the dissociation rate constant, k_6, to the association rate constant, k_5, equals the critical concentration, $\bar{A}_1$ (eq 1). The superscripts

$$\bar{A}_1 = k_6/k_5 = (k_6^B + k_6^P)/(k_5^B + k_5^P) \quad (1)$$

B and P in eq 1 refer to the barbed and pointed ends, respectively.

† From the Department of Cell Biology and Anatomy (J.A.C., E.L.B., S.B.W., and T.D.P.) and the Department of Physiological Chemistry (T.Y.T.), The Johns Hopkins University School of Medicine, Baltimore, Maryland 21205. *Received November 17, 1982.* J.A.C. is a trainee of the Medical Scientist Training Program under National Institutes of Health Grant GM 7309. The research was supported by grants from the NIH (GM-26338) and the Muscular Dystrophy Association of America to T.D.P. and from the National Science Foundation (PCM 8109630) to T.Y.T.

0006-2960/83/0422-2193$01.50/0

Fragmentation is the breaking of an actin filament. Experiments have shown that actin filaments break under the influence of mild solution shear, such as in Ostwald capillary viscometry (Cooper & Pollard, 1982; Tait & Frieden, 1982) or even passage through a Pasteur pipet (Wang & Taylor, 1981). Wegner & Savko (1982) have recently offered evidence that fragmentation occurs in solution during polymerization in the absence of shear, using computerized theoretical models for actin polymerization with and without fragmentation to predict shapes for experimentally observed kinetic polymerization curves. We have confirmed this finding for one ionic condition in this study.

This study focused on the contributions of monomer activation, nucleation, and fragmentation to the overall time course of polymerization. We measured the time course of polymerization, using pyrene-labeled actin fluorescence, as a function of the actin concentration. We chose two ionic conditions under which actin polymerizes, 0.1 M KCl with 1 mM Mg^{2+} and 0.1 M KCl with 0.2 mM Ca^{2+}. We included 0.1 M KCl because of its physiologic relevance. We chose the divalent cation concentrations to vary the speed of polymerization. We analyzed the various steps in polymerization. We made the surprising finding that the actin concentration dependence of the rate of the slow phase was quite low with Mg^{2+}. Computer-assisted analysis of polymerization showed that a monomer activation step was sufficient to explain this novel finding. With Ca^{2+}, monomer activation was not required to account for the kinetics of polymerization, but it was important to include filament fragmentation to obtain a good fit of theoretical models of polymerization with the experimental data. This work was partially presented in preliminary form at the 1982 meetings of the Biophysical Society (Cooper et al., 1982a) and the American Society for Cell Biology (Cooper et al., 1982b).

Materials and Methods

(*1*) *Actin.* Actin was prepared from rabbit skeletal back and leg muscles by the method of Spudich & Watt (1971) and gel filtered on Sephadex G-150 as described by MacLean-Fletcher & Pollard (1980). Actin concentration was determined by absorbance at 290 nm with an extinction coefficient of 2.66×10^4 M^{-1} cm^{-1} (Houk & Ue, 1974). Actin was stored at 4 °C in buffer A (2 mM Tris-HCl, pH 8.0, 0.2 mM ATP, 0.2 mM $CaCl_2$, 0.5 mM dithiothreitol, 0.75 mM NaN_3). For certain experiments, as detailed in the figure legends, actin was dialyzed into buffer A without $CaCl_2$ overnight and used the next day.

(*2*) *Pyrene-Labeled Actin Fluorescence.* Kouyama & Mihashi (1981) reported the preparation of pyrene-labeled actin and observed that its fluorescence increased when it polymerized. We have previously described (Cooper et al., 1983) our preparation and use of pyrene-labeled actin and numerous experiments that documented pyrene-labeled actin fluorescence as a valid assay for actin polymerization. We found that native and pyrene-labeled actin copolymerized both kinetically and at steady state, that pyrene-labeled actin fluorescence corresponded well with light scattering (a proven assay for polymer weight concentration), that pyrene-labeled actin fluorescence was not sensitive to filament length, that bleaching under continuous measurement was minimal, that light levels employed to measure fluorescence did not affect polymerization, and that native and pyrene-labeled actin filaments had the same intrinsic viscosity. These experiments to document the assay were performed under conditions identical with the experiments reported here. Fluorescence was measured in a Hitachi Perkin-Elmer 650-10S spectrofluorometer. We equipped the fluorometer with a brass, water-jacketed cuvette holder (built with the advice and assistance of Dr. Daniel P. Kiehart and Ed Horn) for temperature control, a magnetic stirrer, which was used with a small stir bar in the cuvette below the light path, and a port for injection of fluids into the cuvette with the chamber closed. We usually started an experiment by mixing actin in buffer A with a 10-fold concentrated solution of KCl, imidazole–HCl, pH 7.0, and divalent cation. The stirrer was turned on only for the first few seconds after injection.

(*3*) *Elongation Rate Constants by Electron Microscopy.* We used the method of Pollard & Mooseker (1981) as modified by Dr. Marschall S. Runge and described by Cooper & Pollard (1982). The morphologically identifiable nuclei were actin filaments decorated with chicken muscle myosin subfragment 1 (a gift from Dr. Daniel P. Kiehart), which were fixed with 1 mM glutaraldehyde for 7 min, quenched with 50 mM ethanolamine for 10 min, and separated from these reagents by gel filtration on a short Sephadex G-25 column equilibrated with the buffer for the experiment. These nuclei were stable under the assay conditions, which included ATP. Polymerization rates at the two ends of these nuclei were measured at four concentrations of actin monomer and at one or two time points. Rate constants were obtained from the dependence of the growth rates on actin concentration. The values and errors for the constants were calculated with a least-squares-fit program modified to include the variation of error in input values. The errors in the rates that were input were taken to be the standard deviation of multiple measurements for each concentration.

(*4*) *Calculation of Filament Number from Kinetic Data.* Experimental kinetic curves for actin polymerization were digitized on a Hewlett-Packard 9845B microcomputer with a digitizer and stored on floppy discs. Filament number, N, was calculated from these data with eq 2, the elongation

$$dP/dT = N(k_5A_1 - k_6) \quad (2)$$

equation (Oosawa & Asakura, 1975). A_1 is the actin monomer concentration, which was assumed to be total actin minus polymer. The digitized data was in the form of polymer, P, vs. time, t. dP/dt, the first derivative, was calculated from the digitized data at each time point as $(P_{n+1} - P_n)/(t_{n+1} - t_n)$. The values for the association and dissociation elongation rate constants, k_5 and k_6, respectively, were determined independently by the method described above. With use of these values, the filament number, N, was calculated at each time point, and filament number was plotted vs. time.

(*5*) *Computer Modeling.* Computer programs in Fortran-77 were used to generate kinetic curves through stepwise numerical integration. The computer was a Digital Equipment Corp. PDP-11/34. The program began with initial actin concentration and designated rate constants for elongation, nucleation, monomer activation, and fragmentation. The program made 10 000–300 000 repetitive calculations for time increments of 0.01 or 0.1 s. These increments were determined empirically to be sufficiently short such that the final calculations of polymer vs. time were independent of the value of the time increments. A scheme and relevant equations for a representative model are shown below (Scheme I, eq 3–9). The design and assumptions behind these equations are discussed in the individual sections that follow immediately.

(*A*) *Monomer Activation* (*Eq 3*). When monomer activation was employed in a computer model, we assumed that all actin was unactivated at time zero and then was converted in a first-order reaction to active monomer. Unactivated monomer could not participate in nucleation. For some of the

calculations, we assumed that unactivated monomer could not participate in elongation. The activation process was described by a forward rate constant, k_1, and a backward rate constant, k_2. In general, k_2 was arbitrarily set equal to $k_1/100$. The units of k_1 and k_2 were inverse seconds.

(*B*) *Nucleation.* Several features of the calculations of the nucleation and elongation process were derived from Wegner & Engel (1975). An assumption of steady state was made for the species involved in nucleation. This assumption was technically necessary to make the calculations feasible, and Wegner & Engel (1975) showed that it was a reasonable assumption. Without this assumption, time increments were required to be so small that computer time was orders of magnitude larger. This project would have required several years of computer time. This assumption was also part of the Oosawa & Kasai model (1962). k_3 was the forward nucleation rate constant, and k_4 was the backward rate constant. Units were M^{-1} s^{-1} for k_3 and s^{-1} for k_4. If the size of the nucleus was 3 or greater, the same nucleation rate constants were used for each step that was included in nucleation, such as monomer to dimer, dimer to trimer, trimer to tetramer, etc. Under the steady-state assumption, the ratio of k_3 to k_4 is the only relevant term as long as the constants are large relative to the time increment employed. We arbitrarily set k_4 equal to 500 after determining that this value would meet the assumption that the small oligomers rapidly reach a steady-state concentration. Values of k_4 greater than 500, in conjunction with concomitant increases in k_3, did not change the shape of the polymer vs. time curve. We only varied k_3 as a means of changing the nucleation rate. We used models with several different sizes of nuclei, from dimer to hexamer. The steady-state assumption allows the calculations of concentrations of the nucleating species from the concentration of other species, as shown in eq 4 and 5, instead of in the stepwise fashion employed for other steps. The derivation of eq 5 requires the assumption that A_3 equals A_4 (Wegner & Engel, 1975).

(*C*) *Elongation.* We assumed that elongation occurred from species of the nucleus size and greater. In the calculations, we again used the approach of Wegner & Engel (1975) and assumed that the concentration of the species one protomer larger than the nucleus was equal to the concentration of the nucleus. This assumption was required to make the calculations feasible, given the speed of the computer, and was justified by Wegner & Engel (1975). Without this assumption, one must calculate the rates for each polymer species with a different length. There were more than 1000 such species typically, which increased computer time by 1000 times. The rate of filament number, N, formation was then the rate of nucleus formation (eq 6), and the rate of polymer weight, P, formation was given by the classic elongation equation (eq 8). k_5 was the forward elongation rate constant, and k_6 was the backward elongation rate constant. These rate constants were the sum of the respective rate constants for the barbed and pointed ends. k_5 was always 10^7 M^{-1} s^{-1}. k_6 was 2 s^{-1} for Mg^{2+} models and 6 s^{-1} for Ca^{2+}, on the basis of several measurements of the elongation rate constants and critical concentrations.

(*D*) *Fragmentation.* Fragmentation was introduced (eq 7) by increasing the number of filaments by an amount proportional to the number of filaments, the value of the time increment, a fragmentation constant, F, and the length of the filaments (calculated as total polymer divided by filament number) to some power that was generally 2. The value of 2 was chosen because it usually gave the best fit of the experimental data to the theoretical models as compared to other small numbers such as 0, 1, and 3. The fragmentation constant, F, was an arbitrary coefficient chosen to introduce filament breakage into the scheme. $F = 0$ implied no fragmentation. The units of F were inverse seconds.

Scheme I

$$A_0 \underset{k_2}{\overset{k_1}{\rightleftharpoons}} A_1$$

$$A_1 + A_1 \underset{k_4}{\overset{k_3}{\rightleftharpoons}} A_2$$

$$A_2 + A_1 \underset{k_4}{\overset{k_3}{\rightleftharpoons}} A_3$$

$$A_3 + A_1 \underset{k_6}{\overset{k_5}{\rightleftharpoons}} A_4$$

$$A_4 + A_1 \underset{k_6}{\overset{k_5}{\rightleftharpoons}} A_5$$

In this model the nucleus size is a trimer. Unactivated monomer is A_0, active monomer is A_1, dimer is A_2, trimer is A_3, tetramer is A_4, and pentamer is A_5. The rate constants are defined under Materials and Methods. The related equations for Scheme I are shown below. The variables are as follows:

$$\text{activation: } \Delta A_0 = \Delta T(k_2A_1 - k_1A_0) \quad (3)$$

$$\text{nucleation: } A_2 = (k_3A_1^2 + k_4A_3)/(k_4 + k_3A_1) \quad (4)$$

$$\text{nucleation: } A_3 = k_3A_2A_1/(k_4 + k_5A_1 - k_6) \quad (5)$$

$$\text{nucleation: } \Delta N = \Delta T(k_3A_2A_1 - k_4A_3) \quad (6)$$

$$\text{fragmentation: } \Delta N = \Delta TNF(P/N)^2 \quad (7)$$

$$\text{elongation: } \Delta P = \Delta TN(k_5A_1 - k_6) \quad (8)$$

$$A_1 = A_t - A_0 - 2A_2 - 3A_3 - P \quad (9)$$

A_0, unactivated monomer concentration; A_1, active monomer concentration; A_2, dimer concentration; A_3, trimer concentration; N, polymer number concentration; P, polymer weight concentration (mol of actin protomers/L); ΔT, time increment for the repetitive calculations; A_t, total actin concentration; F, fragmentation constant; k's, rate constants defined under Materials and Methods.

(*E*) *Fit.* The goodness of fit of the theoretical model to the experimental data was calculated for certain analyses. The experimental data were derived from actual experimental kinetic curves produced by the time course of actin polymerization assayed by pyrene-labeled actin fluorescence. We generally used curves at five different actin concentrations under the same ionic conditions. The actin concentrations varied from 5 to 25 μM. The curves were digitized on a Hewlett-Packard 9845B to generate about 150 points per curve, and the data were transferred to the DEC PDP-11 for calculations. The experimental curves were compared to theoretical kinetic curves generated by computer-assisted calculations from a specific model, as described above. Each experimental point was matched with a theoretical point with the same value for time. The error quantity was defined and calculated as the sum over all the points of the squares of the differences between the experimental and theoretical value for the fraction of total polymer that had formed. This program was used to search for the best fit for the experimental data within the limits of a given model by systematically changing the available constants within the model until the error quantity reached its minimum. The program stopped the fit search when the constants could not be varied by 2% and yield a better fit (smaller error quantity) than the one in hand. For several cases, we allowed variations down to 0.01% and found

Table I: Elongation Rate Constants[a]

		assocn ($\times 10^{-6}$ s^{-1} M^{-1})		dissocn (s^{-1})	
Mg^{2+}	Ca^{2+}	barbed	pointed	barbed	pointed
1 mM	0.2 μM	6.9 ± 3.3	1.1 ± 0.6	−3.3 ± 6.1	−0.4 ± 1.6
1 mM	0.2 mM	10.2 ± 2.1		7.0 ± 3.6	
0	0.2 mM	9.5 ± 2.4	1.1 ± 0.2	4.2 ± 3.7	0.8 ± 0.3
		7.9 ± 1.9		5.3 ± 3.7	

[a] Errors shown are one standard deviation. The table lists the Mg^{2+} and Ca^{2+} concentrations and gives the association and dissociation rate constants at the barbed and pointed ends. Conditions: 0.1 M KCl, 20 mM imidazole-HCl, pH 7.0, 0.2 mM ATP, 25 °C.

no significant decrease in error quantity.

Results

(I) Experimental Measurements. The goal was to identify under two different ionic conditions the kinetic steps in actin polymerization and to determine the values of the polymerization parameters. The conditions were 0.1 M KCl with 1 mM Mg^{2+}, where polymerization was rapid (Figure 1A), and 0.1 M KCl with 0.2 mM Ca^{2+}, where polymerization was slow (Figure 1B). For certain experiments, we varied the divalent cation concentration more widely.

(A) Elongation Rate Constants. The elongation process was similar, with small differences, for the two ionic conditions. We examined the elongation process using three different approaches.

First, we quantitatively measured the elongation rate constants for association and dissociation at the barbed and pointed ends of the filaments using electron microscopy, as performed by Pollard & Mooseker (1981). Table I lists the values for the elongation rate constants determined for three ionic conditions with different Ca^{2+} and Mg^{2+} concentrations all with 0.1 M KCl. Within limits of error, the elongation rate constants were the same for all conditions. For the highest ratio of Mg^{2+} to Ca^{2+}, the dissociation rate constant may have been smaller, which was confirmed by the critical concentration measurements.

The second approach was to use the critical concentration as a measure of the ratio of the association and dissociation elongation rate constants (eq 1). From several experiments, the critical concentration was 0.2 μM in 1 mM Mg^{2+} with 0.1 M KCl and 0.6 μM in 0.2 mM Ca^{2+} with 0.1 M KCl, a difference of 3-fold. The critical concentration was the transition point of a plot of pyrene-labeled actin fluorescence vs. total actin concentration. The accuracy of the measurement of the elongation rate constants allowed us to conclude that the association rate constant, k_5, was not 3-fold higher. However, the dissociation rate constant, k_6, might easily have been lower by a factor of 3 and remained within limits of error. Therefore, the lower critical concentration in Mg^{2+} was probably attributable to a lower k_6. This interpretation was used in assigning the values for the association and dissociation elongation rate constants in our computer modeling studies. $k_5 = 10^7$ M^{-1} s^{-1}. $k_6 = 2$ s^{-1} for Mg^{2+} models, and $k_6 = 6$ s^{-1} for Ca^{2+}. In all cases these were, of course, the sums of the rate constants at the two ends. Such a difference in the elongation rate constants between Mg^{2+} and Ca^{2+} could not explain the difference in the bulk polymerization rates shown in Figure 1.

Third, we examined the effect of the divalent cation on initial rates of actin polymerization nucleated by actin filament fragments. In this experiment pyrene-labeled actin monomers at a low actin concentration (3 μM) just above the critical

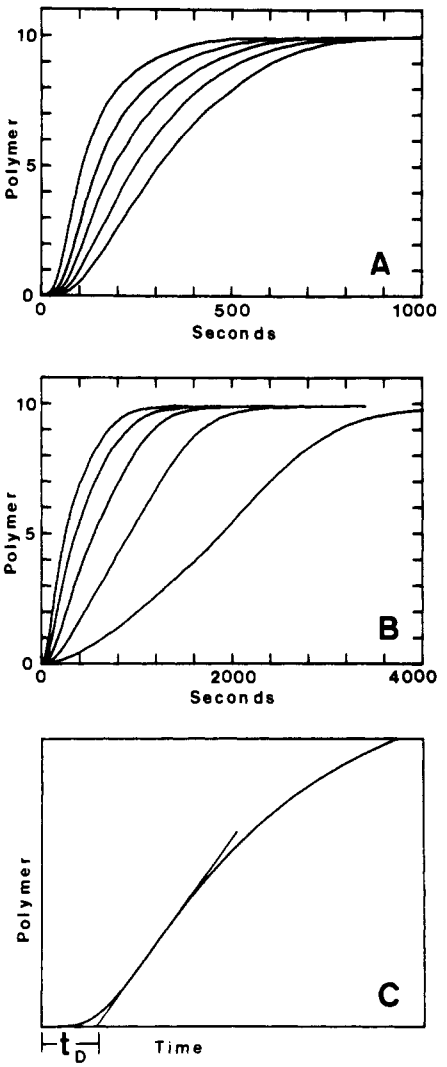

FIGURE 1: Kinetics of actin polymerization. Polymer is normalized units from 0 to 10 plotted vs. time. (A) 1 mM $MgCl_2$, 0.1 M KCl, 20 mM imidazole–HCl, pH 7.0, 90% (v/v) buffer A without $CaCl_2$, 25 °C. The different curves were different actin concentrations, from left to right (μM): 11.8, 9.4, 7.1, 5.9, and 4.7. (B) Conditions similar to those of (A) except that 1 mM $MgCl_2$ was replaced by 0.2 mM $CaCl_2$. Actin concentrations, left to right (μM): 28.3, 23.6, 18.9, 14.2, and 9.4. (C) Delay time. For determination of the delay time, the tangent through the inflection point of the curve was drawn. The x intercept of the tangent was the delay time.

concentration were placed in a cuvette in polymerization buffer that included 0.1 M KCl, 20 mM imidazole–HCl, pH 7.0, and either 1 mM $MgCl_2$ or 0.2 mM $CaCl_2$. Native actin filaments in the experimental polymerization buffer were rapidly injected from a port outside the fluorometer. The fluorescence increased immediately, reflecting the elongation of pyrene-labeled monomers from the native filaments. In a control experiment, the monomers alone did not polymerize at all over the time course employed. We measured the initial slope of the curve, which represented an elongation rate. Ca^{2+} and Mg^{2+} gave the same results within our limits of error as determined by repetitive experiments. Furthermore, the rates were the same when the filaments were added from zero time up to 5 min after the pyrene-labeled actin monomers were mixed with polymerization buffer including Mg^{2+}.

(B) Slow Phase. The events that occur during the slow phase at the onset of polymerization are not accessible to direct measurement like elongation. The kinetic polymerization curve in which the slow phase is observed is a complex function of both time and actin concentration. There is no simple

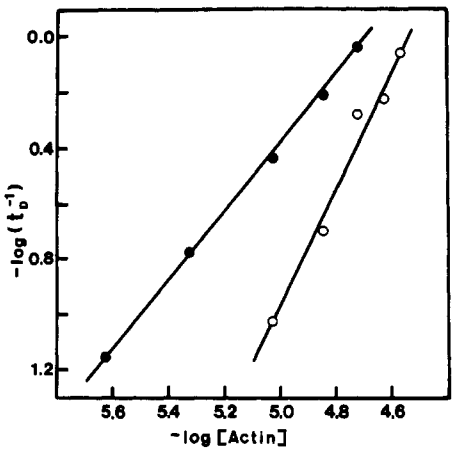

FIGURE 2: A typical log rate vs. log actin concentration plot. The rate of the slow phase in Mg^{2+} and Ca^{2+} was defined as the inverse of the delay time. Divalent cation concentrations: (open circles) 0.2 mM $CaCl_2$; (filled circles) 1 mM $MgCl_2$ and 0.2 mM $CaCl_2$. The addition of Mg^{2+} increased the rate and decreased the slope of the log/log plot. Plots similar to these were used to generate the slopes shown in Table II. Other conditions: 0.1 M KCl, 20 mM imidazole–HCl, pH 7.0, 90% (v/v) buffer A without $CaCl_2$, 25 °C.

Table II: Slopes of Plots of log Rate vs. log Actin Concentration[a]

Mg^{2+}	Ca^{2+}	slope	% label
10 mM	0.6 μM	1.11	10
		1.17	10
1 mM	0.6 μM	1.17	53
		1.23	53
		1.08	33
		1.01	10
		1.33	10
1 mM	0.2 mM	1.34	40
		1.17	28
		1.22	6
0	0.2 mM	2.18	40
		1.87	28
		2.45	10
		2.49	10
		2.14	6

[a] The rate is the inverse of the delay time (Figure 1C). The table lists the Ca^{2+} and Mg^{2+} concentrations, the slope of the log/log plot, and the percentage of the actin that was pyrene-labeled actin as compared to native actin. Conditions: 0.1 M KCl, 20 mM imidazole-HCl, pH 7.0, 0.2 mM ATP.

mathematical description of this curve that might allow one to extract information about the slow phase. We used a computer to perform stepwise numerical integration and calculate this curve for a given theoretical model in which such information about the slow phase was specified by us. We experimentally measured the kinetics of actin polymerization for five different actin concentrations (Figure 1A,B). We then compared experimental and theoretical curves.

Experimentally, we tested the effects of divalent cations on the slow phase by defining the rate of the slow phase as the inverse of the delay time for polymerization (defined in Figure 1C). The rate of the slow phase (inverse delay time) was faster in Mg^{2+} than in Ca^{2+} (Figure 2). This figure also shows how the rate of the slow phase depended on the actin concentration in Mg^{2+} or Ca^{2+}. In both cases plots of log inverse delay time vs. log actin concentration were linear, but the slope was lower for Mg^{2+} than for Ca^{2+}. Table II lists the slopes of the log rate vs. log actin plots for four different concentrations of Mg^{2+} and Ca^{2+}. The slope approached 1 when Mg^{2+} was in great excess of Ca^{2+}. The interpretation of the slope is discussed below in section II.A.1. In addition to our previous control

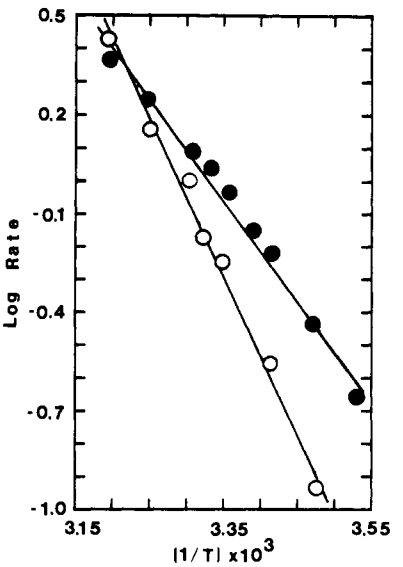

FIGURE 3: Arrhenius plots of the rate of the slow phase. Log rate (inverse delay time) is plotted vs. inverse temperature (K): (open circles) 0.2 mM $CaCl_2$, 16.5 μM actin (28% pyrene label), and 47% (v/v) buffer A without $CaCl_2$; (filled circles) 1 mM $MgCl_2$, 12 μM actin (28% pyrene label), and 33% (v/v) buffer A without $CaCl_2$. Other conditions: 0.1 M KCl, 20 mM imidazole–HCl, pH 7.0. The activation energies, calculated as $E_a = -2.3R$ (slope), where R is the gas constant, are 22.2 kcal/mol for Ca^{2+} and 13.5 kcal/mol for Mg^{2+}.

experiments documenting the validity of pyrene-labeled actin fluorescence as an assay for actin polymerization (Cooper et al., 1983), we performed another control in this set of experiments by determining these slopes with preparations of actin with different ratios of pyrene to native actin. The percentage of pyrene-labeled actin had no effect on the slope (Table II).

To further characterize the difference between Mg^{2+} and Ca^{2+} on the slow phase of polymerization, we examined the temperature dependence of the rate of the slow phase, as defined by the inverse of the delay time, in 0.1 M KCl with Mg^{2+} or Ca^{2+}. Figure 3 shows Arrhenius plots from these data. The activation energies, calculated from the slopes of these plots, were 13.5 kcal/mol for Mg^{2+} and 22.2 kcal/mol for Ca^{2+}. A lower activation energy for Mg^{2+} agreed with the observation that the rate of the slow phase was faster with Mg^{2+}.

(C) Initial Rate Kinetics. Using digitized data from experimental kinetic curves for actin polymerization, we derived plots of filament-number concentration vs. time. The rate of nucleation should be equal to the rate of filament-number formation. As explained under Discussion, plots of log initial rate vs. log actin concentration should have a slope equal to the size of the nucleus [derived from Oosawa & Kasai (1962)]. There were two major problems with this experiment. First, plots of filament number vs. time were concave up (Figure 4), instead of linear or concave down, as would be predicted by a simple model without activation or fragmentation. This result can be explained by the existence of either activation or fragmentation or the invalidity of the steady-state assumption. Second, we attempted to measure the initial rate by extrapolating the slope to time zero. These measurements were highly imprecise and yielded nonlinear plots of log rate vs. log actin. We concluded that this approach was not useful with this method of solution mixing and data collection.

(II) Computer Modeling of Experimental Data. We used computer modeling to assist with the interpretation of the slopes of the log/log plots (Table II), which provided evidence for the existence of an activation step. We used the general

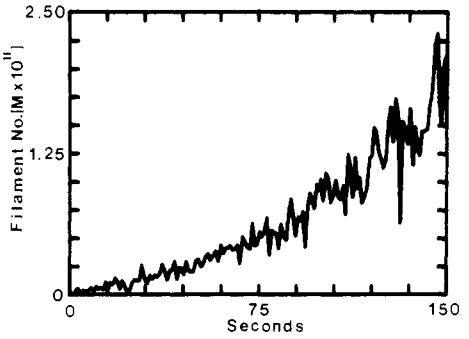

FIGURE 4: Kinetics of filament number vs. time at start of polymerization. Filament number was calculated from digitized curves of polymer vs. time as described under Materials and Methods. The curve is concave up, even at this early time. The total extent of polymerization at 150 s was approximately 0.05 μM. Conditions: 5.9 μM actin (97% pyrene label), 1 mM $MgCl_2$, 0.1 M KCl, 20 mM imidazole–HCl, pH 7.0, 90% (v/v) buffer A, 25 °C.

Table III: Slopes of log Inverse Delay Time vs. log Actin Concentration Plots for Theoretical Models without Activation[a]

nucleus size	slope
dimer	1.5
trimer	2.0
tetramer	2.5
pentamer	3.0
hexamer	3.5

[a] We generated kinetic polymerization curves for several actin concentrations for each nucleus size listed. From each curve, we measured the delay time. We calculated the slope of the log inverse delay time vs. log actin concentration plot. These results were the same for a wide range of nucleation rate constants and actin concentrations, which encompassed our range of experimental results.

model described under Materials and Methods that included monomer activation, nucleation, elongation, and fragmentation. Starting with the general model, we varied the presence or absence of activation, the size of the nucleus, the presence or absence of fragmentation, and values of the rate constants for activation, nucleation, and fragmentation. The elongation rate constants (k_5 and k_6) were measured directly (section I.A.). The computer performed stepwise numerical integration to calculate the time course of polymer formation with a given set of parameters. From these theoretical curves, we calculated the delay times and slopes of log inverse delay time vs. actin concentration (section II.A). We also varied the parameters in the model until a single set of rate constants gave theoretical curves that best matched the experimental curves for five actin concentration (section II.B). We calculated the goodness of fit for each model and in some cases could determine that certain models were significantly better than others.

(A) Analysis of log/log Plots. (1) Activation. In the absence of activation, the slope of plots of log inverse delay time vs. log actin concentration depended on the nucleus size (Table III). The slope was not equal to the size of the nucleus, and no model had a slope of 1.0–1.3 like real actin in Mg^{2+} (Table II). When an activation step was included in the mechanism, models of any nucleus size had a slope of 1.0, given an appropriate choice of rate constants. The slope of the log/log plot was a complex function of nucleus size and the rate constants for activation, nucleation, and fragmentation (Figure 5, Table IV). For example, Figure 5 shows for a dimer nucleus how the slope of the log/log plot depended on the ratio of nucleation to activation rate constants. When the ratio was very small (activation fast, nucleation slow), the slope was 1.5 (see also, Table III). As activation was made slower (k_1 decreased) and nucleation was made faster (k_3 increased),

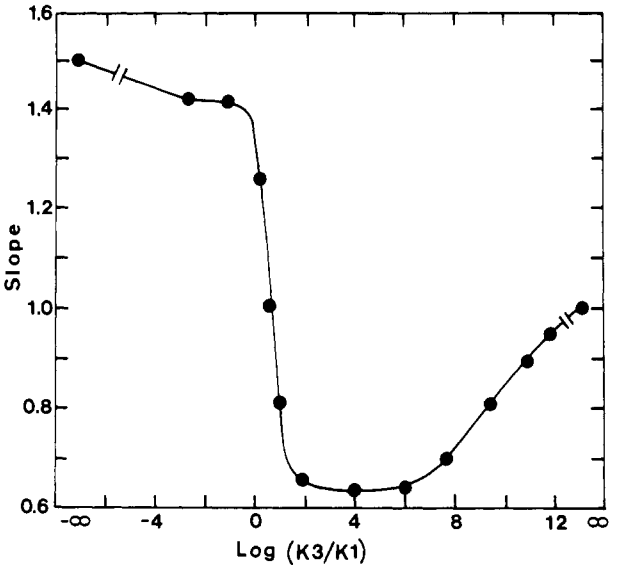

FIGURE 5: Effect of activation on theoretical log/log slope. The slope of the log rate (inverse delay time) vs. log actin concentration plot is plotted against the log ratio of k_3, the forward nucleation rate constant, to k_1, the forward activation rate constant. We varied the rate constants to examine the behavior of the log/log slope when activation and nucleation contributed to the rate-limiting step of the slow phase. In this example the nucleus was a dimer. The rate constants were constrained to yield a certain reasonable value for the delay time for one actin concentration. At the extreme left, log (k_3/k_1) is negative infinity, which indicates that activatioin was relatively very fast and nucleation was relatively very slow. The slope of the log/log plot was 1.5. This result is included in Table III under dimer. At the extreme right, log (k_3/k_1) is positive infinity, which indicates that activation was relatively very slow and nucleation was relatively very fast. The slope of the log/log plot was 1.0, as it was for all other models where activation was solely rate limiting. Surprisingly, between these two extremes the slope fell to a value below 1.0 with a minimum of 0.62.

Table IV: Effect of Activation and Fragmentation Steps on Slopes of log Rate (Inverse Delay Time) vs. log Actin Concentration[a]

		fragmentation	
nucleus size	activation	absent	present
dimer	present	1.12	1.22
	absent	1.44	1.48
trimer	present	1.05	1.25
	absent	1.94	2.43
tetramer	present	1.04	1.26
	absent	2.42	3.34

[a] Values of the slope of log rate vs. log actin concentration are shown for various theoretical models of different size nucleus. The actual rate constants for nucleation and, where present, activation and fragmentation were chosen by a computerized fit routine that minimized the error between the theoretical points and the experimental points of data set 1, which included five actin concentrations. This fit routine included a bias of 6:1 in favor of early as opposed to later points to optimize the fit at early times, which determines the delay time. The experimental slope of the log/log plot for this data set was 1.17.

the slope fell below 1 to a minimum of 0.62 and increased back up to 1 when activation was the sole rate-limiting reaction. For all models of other nucleus size, the results were similar in that the curve decreased from the appropriate value given in Table III to 1, went below 1, and returned back to 1 as activation became rate limiting. The experimental slope in Mg^{2+} was 1.0–1.3. This analysis shows that an activation step was sufficient to predict such a result. The Mg^{2+} experimental data likely fell in the middle of the theoretical plot of Figure 5 because the slope approached 1 from a value of 2–2.5 when

Mg^{2+} was substituted for Ca^{2+}. For the Ca^{2+} experimental data the slope of the log/log plot was 2–2.5. An activation step was not required to predict this result (Table III).

(*2*) *Fragmentation.* The addition of fragmentation to any model without or with activation never lowered the slope of the log/log plot (Table IV). Fragmentation always increased the slope of the log/log plot.

(*B*) *Computer Fit of Theoretical Models to Experimental Data.* In the previous section, we asked whether a theoretical model could predict one single parameter, the slope of the log/log plot, derived from experimental curves of polymerization at different actin concentrations. In this section, we asked how well a theoretical model could predict the entire curve for polymerization of several actin concentrations. We assessed the goodness of fit of theoretical with experimental curves by calculating an error quantity, defined as the sum of squares of the differences between the theoretical and experimental curves at approximately 150 points along each curve for five different curves, each representing a different actin concentration. We determined, for example, if a model with fragmentation was better than a similar model without fragmentation by determining if the error quantity for the former model was significantly less than the error quantity for the latter model. A significant difference in the error quantity was calculated by propagating a reasonable estimate of the error (1–2%) in our experimental measurements through the calculation of the error quantity.

(*1*) *Fragmentation.* Fragmentation improved the fit for the Ca^{2+} data. Wegner & Savko (1982) described experimental kinetic curves for actin polymerization that were simulated well by models that included fragmentation of actin filaments. These curves had a sharp corner in the upper, concave-down portion of the sigmoidal curve of the time course. Our experimental data for polymerization in 0.1 M KCl with Ca^{2+} also displayed such a sharp corner, most notably at low actin concentrations, where the influence of fragmentation should be most noticeable. In all of our theoretical models for actin polymerization with highly varied parameters for nucleation and activation, no curve ever had such a sharp corner in that portion of the curve. The addition of fragmentation to the theoretical model did produce such a sharp corner. Also, the addition of fragmentation to the theoretical model significantly improved the fit of the theoretical model to the experimental kinetic curves for actin polymerization with Ca^{2+}. For example, in one set of experiments where actin polymerization was measured at five actin concentrations with digitization yielding 140 points per curve, the computer fit program varied the available constants and found the best fit for several different models of different nucleus sizes, with and without activation and with and without fragmentation. For each model, the inclusion of fragmentation significantly improved the quality of the fit. The best fit of all the models was one with a trimer nucleus, with no activation, and with fragmentation. For this model, the error quantity calculated between the experimental and theoretical points was 22. The best fit for a similar model without fragmentation had an error quantity of 205. Given a reasonable estimate of the error in our experimental measurements, a difference of 10–20 in the error quantity was a significant improvement. The improvement in the fit is readily observed by inspection of these two theoretical curves and the experimental curve at each of the five actin concentrations employed, three of which are shown in Figure 6. In 0.1 M KCl and 1 mM Mg^{2+}, the addition of fragmentation improved the fit but not by a significant amount.

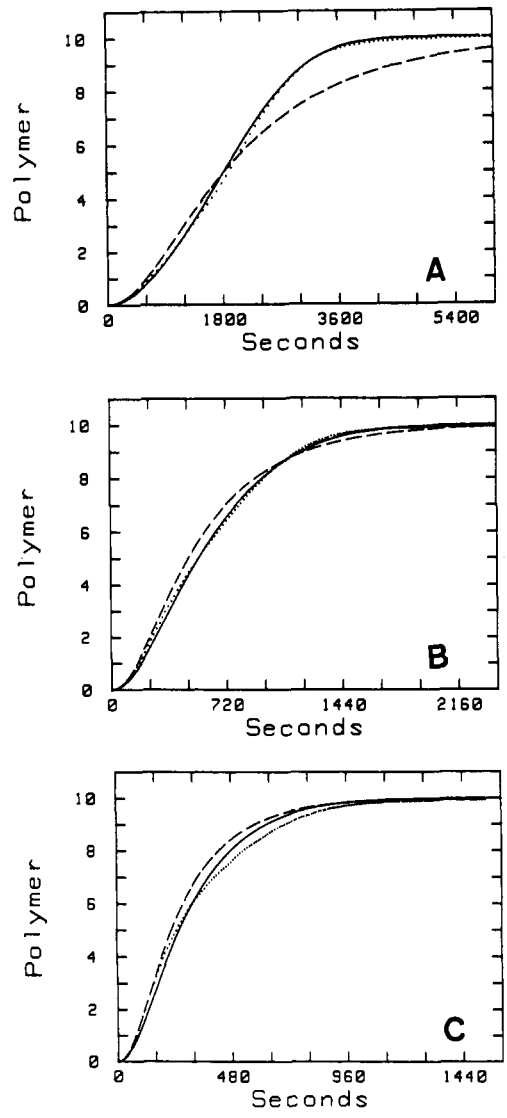

FIGURE 6: A comparison of one set of experimental data in 0.1 M KCl with 0.2 mM Ca^{2+} to theoretical models with and without fragmentation steps. Polymer in arbitrary units from 0 to 10 is plotted vs. time in seconds. The dotted line is experimental data (data set 1); the solid line is the theoretical curve predicted by the best model, with fragmentation; and the dashed line is the theoretical curve for the same model but without fragmentation. For each model, the rate constants were chosen to optimize the fit between the experimental data from five actin concentrations and the theoretical curves. The best model was chosen as described in the text. The figure shows three actin concentrations. Two other concentrations, between the three, are not shown. (A) 9.44 μM actin; (B) 18.88 μM actin; (C) 28.32 μM actin. In each case, the model with fragmentation fits better than the model without fragmentation. The difference between the two models is most pronounced at low actin concentration, where nucleation is slow and the effect of fragmentation on filament number is most noticeable. Fragmentation was proportional to the square of the length, as in eq 7. Conditions: 0.2 mM $CaCl_2$, 0.1 M KCl, 20 mM imidazole–HCl, pH 7.0, 90% (v/v) buffer A without $CaCl_2$, 25 °C.

(*2*) *Models and Parameters of Best Fits.* (*a*) *Mg^{2+} Data.* Table V shows the models with the relevant parameters that gave the best fit to the experimental data for two different actin preparations. The trimer nucleus model is given. For both preparations, trimer was not significantly better than dimer, but trimer was significantly better than tetramer. Fragmentation is listed as absent because models with fragmentation did not give a significantly better fit than models without fragmentation, although models wtih fragmentation did give a better fit than models without fragmentation. The addition of an extra parameter had to yield a fit at least as good as the

Table V: Models and Parameters of Best Fits to Experimental Data[a]

	Mg^{2+} Data	
data set 1	nucleus: trimer fragmentation: absent activation: present	$k_3 = 7900\ M^{-1}\ s^{-1}$ $k_1 = 0.65\ s^{-1}$
data set 2	nucleus: trimer fragmentation: absent activation: present	$k_3 = 5400\ M^{-1}\ s^{-1}$ $k_1 = 0.025\ s^{-1}$
	Ca^{2+} Data	
data set 1	nucleus: trimer fragmentation: present activation: absent	$k_3 = 430\ M^{-1}\ s^{-1}$ $F = 2.2 \times 10^{-13}\ s^{-1}$
data set 2	nucleus: trimer fragmentation: present activation: absent	$k_3 = 330\ M^{-1}\ s^{-1}$ $F = 2.1 \times 10^{-14}\ s^{-1}$

[a] The fit procedure is explained under Materials and Methods and Results. Each data set included five actin concentrations. The concentrations and conditions are given in the legend to Figure 1. The different data sets represent different actin preparations.

fit without that parameter. Activation is listed as present because of the reasons given above in analysis of the log/log slope. In fact, models with activation did not give a significantly better fit than models without activation when points were equally weighted. We have no estimates of the errors for the values of the parameters and do not know why k_1 was so different for the two preparations. The experimental and theoretical kinetic curves agreed well (Figure 7).

(*b*) *Ca^{2+} Data.* Table V also shows the best models and best parameters for two actin preparations. The trimer nucleus gave a significantly better fit than dimer or tetramer. Activation is listed as absent because models with activation did not give a significantly better fit than models without activation. Fragmentation is listed as present because models with fragmentation gave a significantly better fit than models without fragmentation.

Discussion

We wished to analyze actin polymerization to determine what kinetic steps were present and what the rate constants for each step were. We chose two different ionic conditions, 0.1 M KCl with 1 mM Mg^{2+} and 0.1 M KCl with 0.2 mM Ca^{2+}, for analysis. Polymerization was faster in the former buffer. We considered the processes of monomer activation, nucleation, elongation, and fragmentation. Measurements of elongation rate constants were straightforward. Our results are in general agreement with previous work.

The analysis of monomer activation, nucleation, and fragmentation was not straightforward. The information is contained in the kinetic curve of polymer vs. time; however, one cannot integrate analytically from the rate equations for the individual steps to an equation for polymer vs. time. We did this integration numerically in order to examine the influence of the individual steps on the curve of polymer vs. time.

In one experimental approach, we measured the actin concentration dependence of the rate of the slow phase, defined as the inverse of the delay time (Figure 1C). In 0.1 M KCl with 1 mM Mg^{2+}, plots of log rate vs. log actin concentration were linear with a slope of 1.0–1.3. This result was surprising. In general, slopes of log rate vs. log concentration give the order of a reaction. Nucleation definitely exists (because the critical concentration phenomenon exists) under this condition, but it makes no sense for nucleation to be first order. However, this rate, inverse delay time, was an arbitrary definition and not an actual measured rate, so we considered that this slope might not be the order of the reaction. In fact, calculations

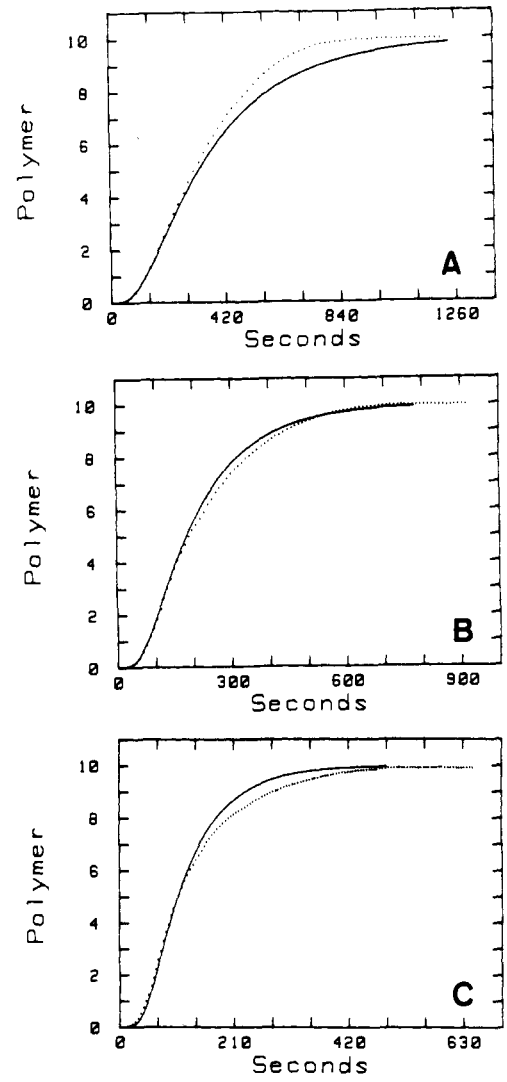

FIGURE 7: A comparison of one set of experimental data in 0.1 M KCl with 1 mM Mg^{2+} to a theoretical model. Polymer in arbitrary units from 0 to 10 is plotted vs. time in seconds. The dotted line is experimental data (data set 1), and the solid line is the theoretical curve predicted by the best model, given in Table V. The choice of the model and actual parameters is discussed in the text. The figure shows three actin concentrations. Two other concentrations, between the three, are not shown. (A) 5.90 μM actin; (B) 8.26 μM actin; (C) 9.44 μM actin. Conditions: 1 mM $MgCl_2$, 0.1 mM KCl, 20 mM imidazole–HCl, pH 7.0, 90% (v/v) buffer A without $CaCl_2$, 25 °C.

of this slope from numerical integration on the basis of theoretical models of different nucleus size (Table III) showed that the slope was not the order of the reaction. Instead, the slope = $(n + 1)/2$, where n was the nucleus size. More importantly, the results in Table III show that no simple model, without monomer activation, predicted a slope of 1.0–1.3, our experimental result for 0.1 M KCl with 1 mM Mg^{2+}. However, when we added monomer activation, models of all nucleus size had a slope of 1.0. Therefore, the presence of a monomer activation step was sufficient to explain the result. Fragmentation was not sufficient to explain the result (Table IV). All modeling studies are subject to criticism that other models, not considered, might also explain the data. We cannot exclude this possibility, but we did test all reasonable models that occurred to us.

Another approach to analyze the slow phase is measurements of initial rates, where assumptions that simplify the mathematics can be made. Oosawa & Kasai (1962) used this approach. They developed a kinetic theory on the basis of their model, and Kasai et al. (1962) performed experiments to

measure the size of the nucleus using certain equations from the kinetic theory. There are some theoretical and experimental difficulties with these results. Oosawa & Kasai first considered the initial rate of polymerization. From their eq 18, reproduced here as eq 10 with our nomenclature, they

$$dP/dt = (k_5A_1 - k_6)\int cA_1^n(t)\,dt \qquad (10)$$

$$dP/dt = bA_1^{n+1} \qquad (11)$$

$$d^2P/dt^2 = k_5cA_1^{n+1} \qquad (12)$$

derived eq 11. We feel that a better solution is to differentiate eq 10 with respect to time, which results in eq 12. In these equations, the variables are as follows: P, polymer weight concentration; t, time; k_5, elongation association rate constant; k_6, elongation dissociation rate constant; A_1, actin monomer concentration; n, nucleus size; b and c, constants. To derive eq 11 and 12 from eq 10, one must assume, as did Oosawa & Kasai (1962), that t is near zero. This implies that A_1 is constant and k_5A_1 is much greater than k_6. Kasai et al. (1962) then measured the initial rate of actin polymerization by Ostwald viscometry at different actin concentrations and plotted log rate vs. log actin concentration to determine n using eq 11. Their result was 3.5. We repeated these experiments and found slopes of 2.5 for conventional (Spudich & Watt, 1971) actin in 0.1 M KCl and 0.2 mM $CaCl_2$, 3.6 for gel-filtered actin in 1 mM Mg^{2+}, 0.1M KCl, and 0.2 mM $CaCl_2$, and 4.6 for gel-filtered actin in 0.1 M KCl and 0.2 mM $CaCl_2$. We were impressed by the difficulty in accurately extrapolating the curves back to time zero to determine the initial rate. Therefore, we attempted to apply the Oosawa and Kasai kinetic theory to initial polymerization kinetics measured by pyrene-labeled actin fluorescence. Combining eq 9 and 10, one generates eq 13 by differentiation. We calculated filament

$$dN/dt = cA_1^n(t) \qquad (13)$$

number, N, vs. time at several actin concentrations. Equation 13 predicted that at early times N vs. t should be concave down or perhaps linear. Our plots were concave up. Our attempts to measure the initial rate and plot log initial rate vs. log actin concentration were also futile because these measurements were highly irreproducible and the plots were not linear. Kasai et al. (1962) also measured the halftime for polymerization, which should be proportional to the actin concentration to a power equal to $n/2$, as shown by the kinetic theory of Oosawa & Kasai (1962). Their result was $n/2$ equal to 1.5. Theoretically, this treatment includes assumptions valid only during the initial phase of polymerization, and experimentally, Ostwald viscometry accelerates polymer formation by shearing the solution and breaking filaments, which was not included in the theory.

Our second major finding was to confirm the finding of Wegner & Savko (1982) that fragmentation can exist in undisturbed solutions. In this analysis we compared the fit between experimental kinetic polymerization curves and theoretical curves generated by computer-assisted numerical integration. For both ionic conditions, the addition of fragmentation to the model improved the fit between theoretical and experimental polymerization curves. For 0.1 M KCl with 0.2 mM Ca^{2+}, the improvement was significant, on the basis of a quantitative calculation of significance. The results are striking to the eye as well (Figure 6). The improvement was not significant for 0.1 M KCl with 1 mM Mg^{2+}. We do not know whether the reason that fragmentation was more important with Ca^{2+} than Mg^{2+} was because filaments with Ca^{2+} were more fragile or simply because nucleation was slower, which made fragmentation more noticeable.

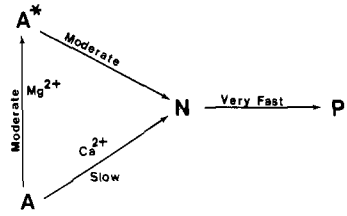

FIGURE 8: A scheme for actin polymerization. This scheme illustrates and summarizes our interpretation of our results for activation and nucleation: A, unactivated actin monomer; A*, activated actin monomer; N, nucleus; P, polymer. In Ca^{2+}, unactivated monomers form nuclei by a slow step. In Mg^{2+}, monomers can be activated to a form for which the nucleation rate is much higher. The elongation step, from nuclei to polymer, is very fast in each case. The scheme is more fully explained under Discussion.

Polymerization was faster in 0.1 M KCl with 1 mM Mg^{2+} than in 0.1 M KCl with 0.2 mM Ca^{2+}. The elongation rate constants were similar, but the nucleation parameters were different. The data for Mg^{2+} were fit well by models with nucleus-size dimer or trimer. The data for Ca^{2+} were fit best by a trimer nucleus. The forward nucleation rate constant, k_3, was 15–20 times larger for Mg^{2+} data than for Ca^{2+} data. The higher nucleation rate constant and the smaller nucleus size agree with the increased bulk rate of polymerization for Mg^{2+} vs. Ca^{2+}.

We can summarize our interpretation of our findings about activation and nucleation in the simple scheme shown in Figure 8. For polymerization in 0.1 M KCl with Ca^{2+}, there is no activation step. The binding of salt and any subsequent transformations that allow actin to polymerize happen too rapidly relative to nucleation to be detected by our approach. Actin nucleates slowly and elongates very rapidly. In 0.1 M KCl with Mg^{2+}, this pathway is still available. However, an alternate faster pathway also exists. Actin monomers can undergo a first-order process, probably a conformational change, to activated monomers, A*. This form undergoes nucleation faster than A. Overall, the time to nucleus formation is less even though another step has been added. The rate of the elongation process is probably the same for activated and unactivated monomer since the elongation rate constants were similar with Ca^{2+} and Mg^{2+} and the elongation rate did not change with time with Mg^{2+}.

Acknowledgments

We are grateful to Drs. Kenneth Johnson, Gary Ackers, and William Harrington for helpful discussion and instruction. Barry Knox helped us with the error calculations for the elongation rate constants. We are grateful to Drs. Susan Craig, Julien Davis, William Harrington, and Daniel Kiehart for reading and criticizing the manuscript.

Registry No. Mg, 7439-95-4; Ca, 7440-70-2.

References

Cooper, J. A., & Pollard, T. D. (1982) *Methods Enzymol. 85*, 182–210.

Cooper, J. A., Tsong, T. Y., & Pollard, T. D. (1982a) *Biophys. J. 37*, 191a.

Cooper, J. A., Walker, S. B., Buhle, E. L., Jr., & Pollard, T. D. (1982b) *J. Cell Biol. 95*, 297a.

Cooper, J. A., Walker, S. B., & Pollard, T. D. (1983) *J. Muscle Res. Cell Motil.* (in press).

Frieden, C. (1982) *J. Biol. Chem. 257*, 2882–2886.

Frieden, C., Lieberman, D., & Gilbert, H. R. (1980) *J. Biol. Chem. 255*, 8891–8893.

Houk, T. W., Jr., & Ue, K. (1974) *Anal. Biochem. 62*, 66-74.
Kasai, M., Asakura, S., & Oosawa, F. (1962) *Biochim. Biophys. Acta 57*, 22-31.
Kouyama, T., & Mihashi, K. (1981) *Eur. J. Biochem. 114*, 33-38.
MacLean-Fletcher, S., & Pollard, T. D. (1980) *Biochem. Biophys. Res. Commun. 96*, 18-27.
Oosawa, F., & Kasai, M. (1962) *J. Mol. Biol. 4*, 10-21.
Oosawa, F., & Asakura, S. (1975) *Thermodynamics of the Polymerization of Protein*, Academic Press, New York.
Pardee, J. D., & Spudich, J. A. (1982) *J. Cell Biol. 93*, 648-654.
Pollard, T. D., & Mooseker, M. S. (1981) *J. Cell Biol. 88*, 654-659.
Rich, S. A., & Estes, J. E. (1976) *J. Mol. Biol. 104*, 777-792.
Rouayrenc, J., & Travers, F. (1981) *Eur. J. Biochem. 116*, 73-77.
Spudich, J. A., & Watt, S. (1971) *J. Biol. Chem. 246*, 4866-4871.
Tait, J. F., & Frieden, C. (1982) *Biochemistry 21*, 3666-3674.
Wang, Y.-L., & Taylor, D. L. (1981) *Cell (Cambridge, Mass.) 27*, 429-436.
Wegner, A., & Engel, J. (1975) *Biophys. Chem. 3*, 215-225.
Wegner, A., & Savko, P. (1982) *Biochemistry 21*, 1909-1913.

Use of 3′-*O*-Naphthoyladenosine 5′-Diphosphate To Probe Distinct Conformational States of Membrane-Bound Adenosine 5′-Diphosphate/Adenosine 5′-Triphosphate Carrier†

Marc R. Block,* Guy J.-M. Lauquin, and Pierre V. Vignais

ABSTRACT: The fluorescent analogue of ADP, 3′-*O*-naphthoyladenosine 5′-diphosphate (N-ADP), which binds to the mitochondrial ADP/ATP carrier but is not transported [Block, M. R., Lauquin, G. J. M., & Vignais, P. V. (1982) *Biochemistry 21*, 5451-5457], has been used to probe the interactions with the ADP/ATP carrier of two specific inhibitors, carboxyatractyloside (CATR) and bongkrekic acid (BA), both in heart mitochondria and in inside-out submitochondrial particles obtained by sonication of mitochondria (sonic particles). The peculiarity of these inhibitors is that they are mutually exclusive for binding; moreover, in mitochondria, CATR attacks the carrier from the outside, and BA from the inside, while in sonic particles the reverse is true. In the present work, the mitochondria and sonic particles were loaded with N-ADP, and the amount of carrier-bound N-ADP released upon addition of CATR and BA was monitored fluorometrically. The kinetics of N-ADP release could be easily resolved by lowering the temperature. In mitochondria, the release was clearly biphasic at 10 °C; the first phase induced by CATR corresponded to the release of 40-70% of the carrier-bound N-ADP and lasted for less than 0.5 s; it ended abruptly and was followed by a very slow release of the rest of the carrier-bound N-ADP, which required more than 20 min for completion. Addition of BA at the onset of the slow phase dramatically accelerated the release of N-ADP; acceleration also occurred upon addition of micromolar concentrations of ADP or any transportable nucleotide. Reversing the sequence of additions, i.e., starting by the addition of BA, led to similar results, namely, a two-step release of the bound N-ADP consisting of a rapid phase of partial release of bound N-ADP followed by a slow one that was accelerated by CATR or ADP. In the case of sonic particles loaded with N-ADP, BA was able to induce the extensive release of the carrier-bound N-ADP at 10 °C, either in the absence or presence of ADP. On the other hand, CATR was inefficient in releasing bound N-ADP at 10 °C, unless ADP or another transportable nucleotide was added. These data provide the first direct experimental evidence in favor of an ADP/ATP carrier model in which the CATR or BA conformations exist prior to the addition of CATR or BA. Any given ADP/ATP carrier unit in the mitochondrial membrane is suggested to exist either in the CATR conformation or in the BA conformation. Bound N-ADP would be released upon binding either of CATR to those carrier units in the CATR conformation or of BA to those in the BA conformation. In heart mitochondria, between 40 and 70% of the carrier units would be in the CATR conformation, depending on the nature of the preparation, the remainder being in the BA conformation. In sonic particles, however, most of the carrier units would be in the BA conformation. The transition between the CATR and BA conformations is very slow at 10 °C; it is increased by raising the temperature or by adding micromolar concentrations of ADP or any transportable nucleotide, suggesting that it is an intrinsic event in ADP/ATP transport.

Previous studies from this laboratory (Block et al., 1982) have led to the characterization of a new fluorescent ligand of the ADP/ATP carrier, namely, 3′-*O*-naphthoyl-1-adenosine 5′-diphosphate (N-ADP).[1] This fluorescent analogue of ADP was able to bind to the ADP/ATP carrier in mitochondria and inside-out submitochondrial particles (sonic particles) but was not transported, in accordance with the well-known specificity of the carrier protein for ADP and ATP (Duée & Vignais, 1969; Boos & Schlimme, 1979). However, N-ADP was found to inhibit ADP transport. The binding of N-ADP to the membrane-bound ADP/ATP carrier and, conversely, its release were associated with opposing changes in the fluorescence intensity, namely, a fluorescence decrease in the case of N-

† From the Laboratoire de Biochimie (CNRS/ERA 903 et INSERM U.191), Département de Recherche Fondamentale, Centre d'Etudes Nucléaires and Faculté de Médecine de Grenoble, 85X, 38041 Grenoble Cedex, France. *Received October 20, 1982.* This work was supported in part by a grant from the Fondation pour la Recherche Médicale.

[1] Abbreviations: sonic particles, inside-out particles prepared by ultrasonic irradiation of beef heart mitochondria; CATR, carboxyatractyloside; BA, bongkrekic acid; AMPPNP, 5′-adenylyl imidodiphosphate; N-ADP, 3′-*O*-naphthoyl-1-adenosine 5′-diphosphate; Mes, 2-(*N*-morpholino)ethanesulfonic acid; EDTA, ethylenediaminetetraacetic acid; FCCP, carbonyl cyanide *p*-(trifluoromethoxy)phenylhydrazone.

0006-2960/83/0422-2202$01.50/0